ACS APPLIED ELECTRONIC MATERIALS

pubs.acs.org/acsaelm

Article

Volume Shrinkage in InPb/Au Solder Joints under Varied Environmental Conditions: A Kinetics Study

Mousa Al-Rbai'eh, Simone Bandini, Alessia Sanna, Luca Sollecchia, Lorenzo Simone, Marco Rossi, Danilo Dini,* and Mirko Rocci*

Cite This: *ACS Appl. Electron. Mater.* 2025, 7, 10161−10171

Read Online

ACCESS | Metrics & More | Article Recommendations

ABSTRACT: The dynamic stability of InPb/Au solder joint volumes under thermal aging has been investigated, exploring the interplay of atmospheric and vacuum conditions. Samples were aged at 25 °C, 85 °C, and 125 °C under atmospheric pressure (10^3 mbar) and at 125 °C in high vacuum (HV) (10^{-6} mbar). Using advanced opto-digital microscopy (ODM), high-resolution X-ray microscopy (XRM), and scanning electron microscopy with energy-dispersive spectroscopy (SEM/EDS), we uncovered significant morphological transformations and pronounced volume shrinkage. These changes were associated with the growth of Au_xIn_y intermetallic compounds together with Pb- and In-rich phases, forming characteristic dark rings at the solder/Au interface. The activation energy (E_a) governing the shrinkage process was precisely determined to lie within 0.38−0.41 eV, consistent with diffusion-controlled migration of In and Pb into Au-rich IMCs, while acceleration factors (AFs) were quantified, enabling long-term behavior prediction. In comparison, SnPb/PtAu and SAC305/ENIG solder joints exhibited negligible volume change and slower IMC growth, highlighting the unique susceptibility of InPb/Au to volumetric variation. These findings reveal the primary influence of temperature and pressure on solder alloy integrity, providing practical insights for reliability assessment in space, aerospace, and other high-reliability electronic applications, where lead is still allowed.

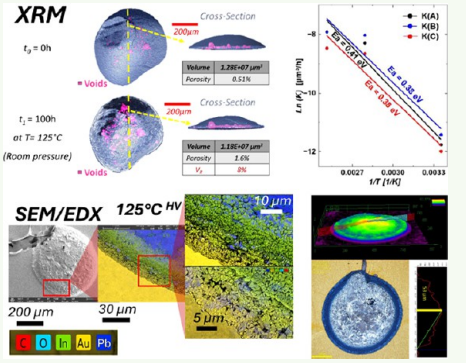

KEYWORDS: *(InPb/Au, solder joints, volume reduction, activation energy, acceleration factors)*

1. INTRODUCTION

Indium−lead (InPb) alloys have gained significant attention in the electronics industry, particularly for the high reliability of the solders on gold (Au), which are used in aerospace and military systems due to the uniqueness of their properties.[1−3] These alloys offer several advantages over traditional tin−lead (SnPb) solders, including similar melting points and superior resistance to thermal fatigue, which are critical in demanding environments.[1,2] The InPb system provides a range of alloy compositions with solidus temperatures from 156.6 °C (pure indium) to 327.5 °C (pure lead). For instance, the composition 50In-50Pb has a melting point of about 210 °C and solidifies at 185 °C. Such thermal characteristics render this eutectic highly suitable for applications requiring controlled melting properties.[1−3] The relatively low melting point of this alloy allows for lower soldering temperatures, thus reducing thermal stress on sensitive components, a significant benefit in high-reliability electronic components. Moreover, InPb solders exhibit significantly reduced Au scavenging behavior compared to SnPb solders, which can rapidly dissolve Au metallization and form hard, brittle $AuSn_4$ intermetallic compounds (IMCs). This makes InPb solders particularly suitable for use with thick gold plating, which is common in military and space applications.

However, the use of InPb solders is not without challenges, including potential corrosion in high-humidity environments and lower mechanical strength compared to SnPb solders. While previous research has extensively investigated the formation of IMCs in InPb solder joints, the specific issue of long-term volume stability, particularly under varying thermal cycling conditions, has not been comprehensively studied.[1,2]

To address this gap, this study aims to quantify and characterize the volume evolution of InPb solder joints on gold-metallized substrates as a function of time, temperature, and initial composition. Our approach utilizes nondestructive evaluation techniques, such as ODM and SEM/EDS for elemental identification and intermetallic compound evaluation, to monitor volume changes in solder joints over extended

Received: July 31, 2025
Revised: October 24, 2025
Accepted: November 2, 2025
Published: November 11, 2025

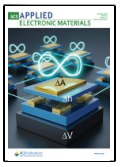

periods at different temperatures, allowing for continuous observation of joint evolution without the need for destructive microscopic analysis. This investigation will contribute to the understanding of InPb solder joint stability. For purposes of benchmarking, SnPb/PtAu solder joints were also tested: they showed no detectable shrinkage, with volumes of solder joints being stable under thermal and vacuum exposure as well as during their IMC evolution.[4−6] Similarly, solder joints of SAC305 on electroless nickel immersion gold (ENIG) finish showed morphological stability with no volume variation and modest growth of IMCs over prolonged high-temperature vacuum and room-pressure exposure.[7−9] In comparison, InPb/Au joints showed progressive volumetric shrinkage and significant IMC growth, highlighting their peculiar susceptibility to harsh environmental conditions. The findings are key for predicting the long-term reliability of InPb solder joints and optimizing their processing for improved performance in harsh environments.[10,11]

2. EXPERIMENTAL SECTION

InPb/Au samples were prepared by European Space Agency (ESA)-certified operators at Thales Alenia Space, Italy. The substrate consisted of Al_2O_3 sequentially coated with a metallic buffer layer, followed by a 6 μm-thick Au top layer. Samples were cut to dimensions of ∼6 × 7 mm^2 and then cleaned with isopropyl alcohol (IPA) and dried using a nitrogen gun to ensure a contaminant-free surface.[12,13]

The InPb alloy (75% In, 25% Pb by weight, sourced from Indium Corp.) was prepared in ribbon form and cut into three size groups: ∼200 μm (A), ∼400 μm (B), and ∼600 μm (C) in diameter. Soldering was performed with a METCAL (mod. MX-5000) soldering station equipped with a UFTC-7CH06 tip, ensuring that the maximum alloy temperature did not exceed 220 °C. The substrate was preheated on a hot plate at 130 °C, and ALPHA RMA-376 solder flux was used to ensure proper wetting and bonding conditions of the InPb alloy.[13]

A total of 12 substrates were prepared, with an equal number of substrates for each of the three solder systems that were researched: InPb/Au, SnPb/PtAu, and SAC305/ENIG. Four substrates were used to represent each alloy system, with every substrate containing nine solder joints. Each substrate was assigned to one of four selected thermal aging conditions: (1) 25 °C at 10^3 mbar, (2) 85 °C at 10^3 mbar, (3) 125 °C at 10^3 mbar, or (4) 125 °C at 10^{-6} mbar. This setup provides a total of 36 joints for each alloy system and 108 joints in total, with a well-balanced and repeatable layout for every type of solder.

These three temperature points were specifically selected to be representative of room storage (25 °C), service conditions (85 °C), and acceleration of stress aging at the maximum reliable limit of InPb solder (125 °C). Experiment durations were conducted for up to 1000 h with intermediate characterizations performed at different time intervals.

Surface morphology analysis via ODM was conducted using an Olympus DSX500 with a 20× objective lens, allowing for high-resolution imaging and volume calculations; all volume measurements were repeated three times per condition, and uncertainty was reported as 2σ based on the repeated data set. XRM analyses were performed using a ZEISS Xradia Versa 610 X-ray Microscope operated at 140 kV and 21 W with a current of 150.1 μA. This nondestructive technique allowed for a detailed study of the material's internal imaging with a spatial resolution down to 500 nm. To estimate IMC composition and elemental segregation, SEM/EDS analyses were consistently performed on selected areas before and after thermal aging.

Figure 1 provides a comprehensive overview of the sample preparation, including (a) an array of InPb alloy on a Au substrate exposed to different environmental conditions, (b) ODM micrographs showing the surface condition of samples with increasing size from A to C, and (c) a schematic cross-section outlining the structure and the chemical composition of the substrate and alloy samples.

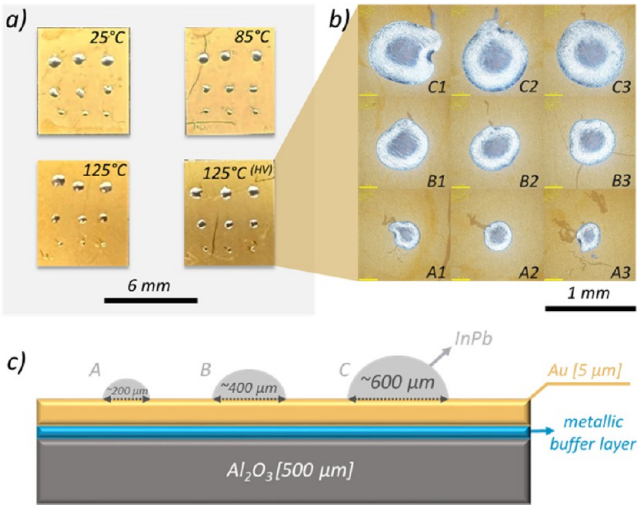

Figure 1. InPb/Au alloy samples fabricated under various thermal aging conditions. (a) Array of InPb alloy on a Au substrate with four replicates to be aged at different temperatures and pressures: 25 °C, 85 °C, and 125 °C at ∼1 × 10^3 mbar and 125 °C at 1 × 10^{-6} mbar. (b) Optical MIX-field micrographs (A1−C3) showing the surface morphology of alloy samples with increasing dimensions. (c) Schematic cross-section of alloy samples A, B, and C.

Junctions of varying sizes were fabricated to explore potential size-dependent morphological evolution with aging time and varying pressure conditions. For benchmarking purposes, solder joints of SnPb/PtAu and SAC305/ENIG were also prepared and characterized using the same protocol, ensuring that volumetric stability and IMC evolution could be directly compared across alloy systems.

3. RESULTS AND DISCUSSION

This section presents our experimental findings on the aging behavior of InPb solder alloys under various conditions. The analysis focused on the kinetics of volume shrinkage and the effects of temperature and pressure on this phenomenon.

3.1. Comparison of ODM and XRM Measurements. A comparison between the ODM and XRM sample mapping is shown in Figure 2a and b. Analyses of small and medium (A2, $B2_{125\ °C}$) sized junctions, at t_0 = 0 h and after t_1 = 100 h of aging at 125 °C and room pressure, were performed as shown in Figure 2c and d, revealing key aspects of our volume measurement techniques and their implications for solder joint characterization. XRM consistently measured volumes larger than those of the ODM, with discrepancies ranging from 22% to 47%. The discrepancy was more pronounced for smaller and medium joints (A2, $B2_{125\ °C}$, Figure 2c and d) and is attributed to XRM's ability to detect internal structures, i.e., a feature that renders it harder to discard any spurious contribution from the substrate in the calculation of the volume. In contrast, the ODM reveals exclusively the morphological features of the surface.

The relevant aspect of this combined analysis is that both microscopy techniques showed consistent trends in volume reduction$V_R = (V_{t>0} - V_{t=0}) > 0]$ over time (Figure 2c and d), validating that shrinkage is a real material response and not a measurement artifact. Besides, XRM revealed increased internal porosity over time, particularly in the $A2_{125\ °C}$ smaller and $B2_{125\ °C}$ medium junctions (Figure 2c and d). Quantitatively, porosity rose only from ≈0.5% at t = 0 to

https://doi.org/10.1021/acsaelm.5c01580
ACS Appl. Electron. Mater. 2025, 7, 10161−10171

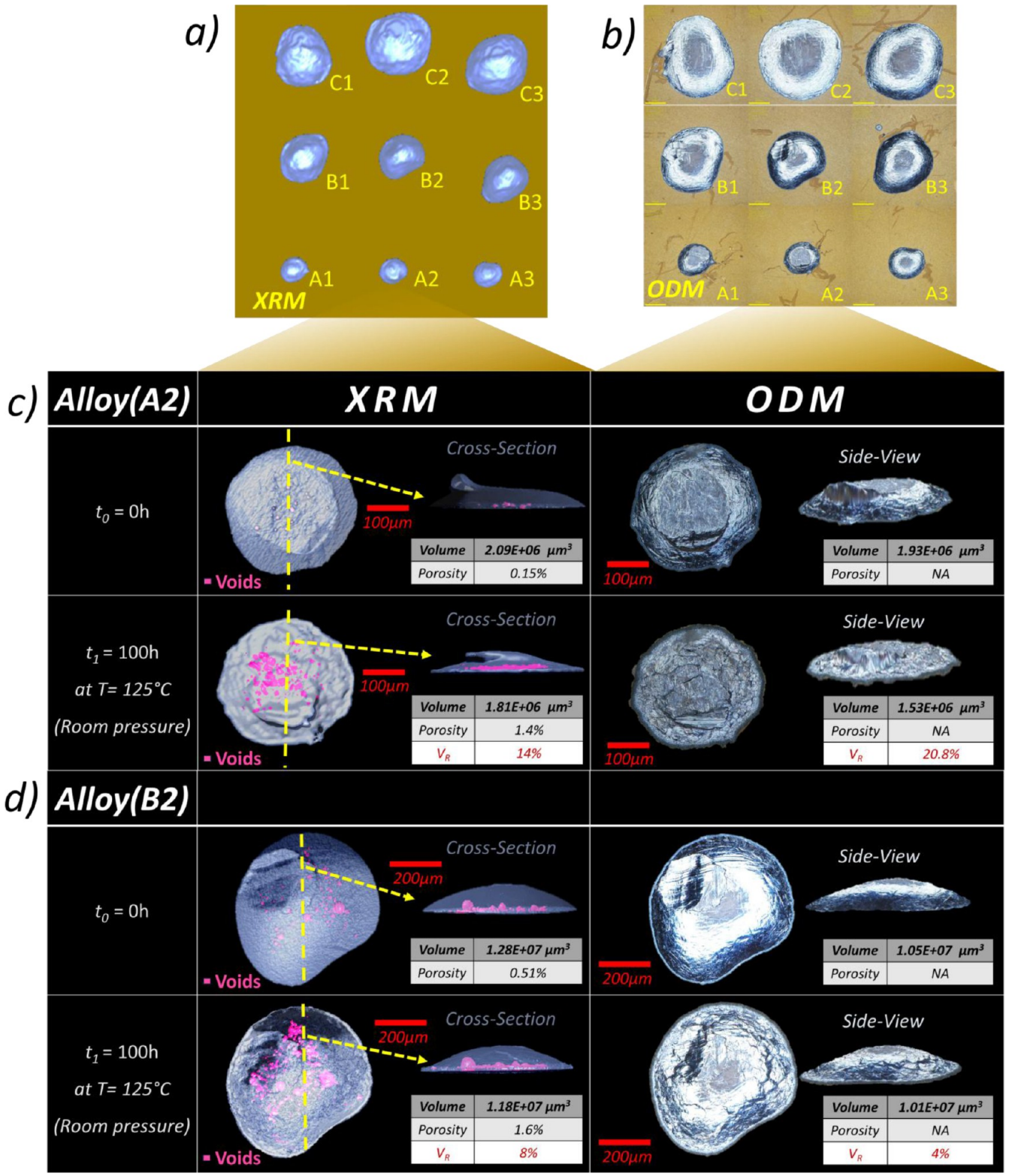

Figure 2. Comparative analysis of InPb solder joints using XRM and ODM: (a) Initial states of nine alloys visualized by XRM; (b) surface morphology of the same alloy samples captured via ODM; (c,d) volumetric comparison of alloy A2 and B2, respectively, at t = 0 and after 100 h of aging at 125 °C at room pressure, using both XRM and ODM techniques.

≈1.6% at t = 1000 h for alloy B2, confirming that void formation cannot account for the measured shrinkage. ODM and XRM thus provide complementary data on surface morphology and internal structure, respectively, offering a comprehensive view of solder joint aging evolution.

These measurements confirm that such volumetric shrinkage is not a result of void growth or mass reduction and hence must be connected with microstructure changes, predominantly the growth and propagation of IMCs, as discussed thoroughly in later sections.

https://doi.org/10.1021/acsaelm.5c01580
ACS Appl. Electron. Mater. 2025, 7, 10161−10171

For the subsequent analyses, we used ODM as it reliably tracks relative volume changes ($\Delta V/V_0$) over time, i.e., the primary focus of this study. The relative changes detected by the ODM closely matched those from the XRM, ensuring an accurate assessment of surface integrity and performance evolution.

3.2. Volume Shrinkage Kinetics: Activation Energy and Acceleration Factor. For the detailed examination of the observed V_R, the standard Arrhenius approach was employed to assess volume shrinkage kinetics, following the methodologies established in previous studies on solder joint aging.[10,14,15] All the samples were subjected to up to 1000 h of aging time to fully characterize the phenomenon. Figure 3

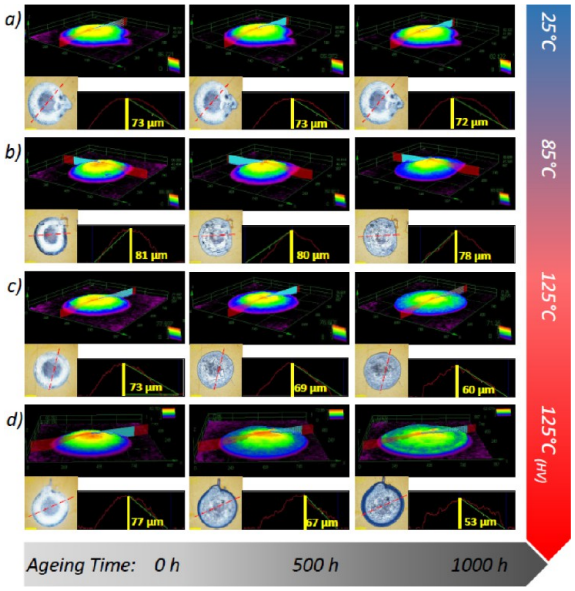

Figure 3. ODM 3D images and profiles showing the morphological evolution as a function of aging time for large C2 InPb/Au alloys at: (a) 25 °C, (b) 85 °C, (c) 125 °C and "room pressure", and (d) 125 °C in HV. Data were collected at 0, 500, and 1000 h. The top rows present false-colored 3D images showing the morphological evolution of the solder alloys (axes in μm). The corresponding line plots beneath each 3D profile display the distribution of thickness across a central cross-section, highlighting a progressive decrease in alloy thickness (in μm) over time.

illustrates the ODM 3D micrographs of InPb/Au solder joints, showing the morphology and profile evolution over the aging time of C2 junctions for each sample aged at 25 °C, 85 °C, and 125 °C in air and at 125 °C in HV conditions. The profiles were taken across the same line of the junctions to ensure proper comparison. Significant profile reduction (up to ~31%, peak-to-peak comparison) and overall morphology degradation were observed after 1000 h, mainly for the junctions aged at 85 and 125 °C (see Figure 3b–d).

Tables 35 show the progressive volumetric shrinkage of InPb/Au solder joints of varying sizes (A to C) with aging time. The findings verify a consistent trend of volumetric reduction, which becomes more significant at elevated temperatures and smaller sizes, thereby establishing a strong temperature- and size-dependent trend.

The elemental composition and the spatial distribution of the interphase formed at the solder/Au junction in different aging stages were analyzed using SEM-EDS. Figure 4 presents the SEM-EDS elemental mapping and provides detailed

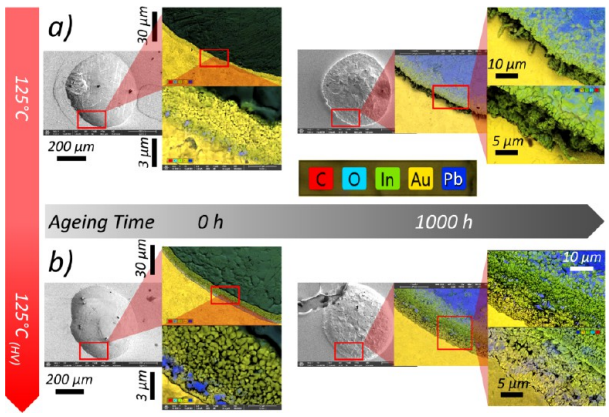

Figure 4. SEM-EDS elemental color mapping of InPb/Au samples aged at 125 °C at ~1 × 10^3 mbar and 125 °C in HV (1 × 10^{-6} mbar) conditions over 0 and 1000 h: Panels (a,b) illustrate the elemental distribution at various stages of aging and evidence the variations in diffusion and segregation behavior of the elements Au, In, Pb, and O. These mappings provide insight into the redistribution of materials across IMCs during aging and complement the morphological data obtained from ODM and SEM analysis.

information on the distribution of the elements at the InPb/Au junction across the sample for various aging times for the B2 sample (medium size), at t_0 = 0 h and after t_1 = 1000 h aged at 125 °C under normal atmospheric pressure (10^3 mbar) and at 125 °C in an HV (10^{-6} mbar).

In Figure 4, at intermediate magnification, open red rectangles mark the sample regions from which SEM-EDS maps were taken. In particular, the diffusion phenomena of Pb and In over aging time were observed. Pb generally diffuses toward the bulk of the solder with time, whereas In migrates outward with a tendency to accumulate at the border, thus forming IMCs with Au. In the vacuum-aged sample, the growth of the IMC layer appeared more uniform, likely due to the absence of oxygen, which limits oxidation and allows for more stable and homogeneous diffusion across the interface. Another observation is in region 4 of Table 1, where the Au:In ratio approaches Au_7In_3. This observation is supported by the EDS analysis shown in Figure 5 and the associated phase prediction based on the data shown in Figure 6. One of the main goals of this study was to verify the formation of AuIn2, a stable phase previously reported by Yost.[11] This was successfully confirmed in the air-aged sample: Region 2 in Table 2 shows $AuIn_2$ which corresponds to the atomic percentage. This composition is also supported by the EDS mapping and spectra shown in Figures 7 and 8 and Tables 3–5.

Figure 9 shows the volume measurements performed by the ODM every 80–100 h of aging time on all small, medium, and large solder joints (respectively classified as A, B, and C samples) and averaged for each size. A systematic volume shrinkage of up to 31% over aging temperature and time was confirmed by the observations.

The progressive shrinkage of the InPb/Au joints can be attributed to densification arising from the transformation of the solder matrix into compact Au–In intermetallic compounds (mainly $AuIn_2$ and Au_7In_3). Therefore, the origin of the shrinkage effect must be sought in the eventual formation of IMCs (not considered an oxidative degradation product), which may result in a denser crystalline structure compared to that of the original solder alloy.

https://doi.org/10.1021/acsaelm.5c01580
ACS Appl. Electron. Mater. 2025, 7, 10161–10171

Table 1. Summary of Atomic % of InPb Solder Joint on Au after 1000 h at 125 °C in HV

	Atomic %								
Element	Region 1	Region 2	Region 3	Region 4	Region 5	Point 1	Point 2	Point 3	Point 4
C	8.6	4.4	8.8	9.5	9.0	2.7	6.9	4.3	6.2
O	37.3	25.5	18.3	16.6	11.7	10.9	17.4	13.2	15.7
In	6.4	23.9	37.5	18.7	2.1	46.6	14.2	45.2	20.5
Au	7.6	18.1	26.3	43.7	71.9	30.4	15.0	31.3	50.9
Pb	40.2	28.0	9.0	11.5	5.3	9.4	46.4	6.1	6.7
In:Au	1:1	4:3	3:2	3:7	1:34	3:2	1:1	3:2	2:5

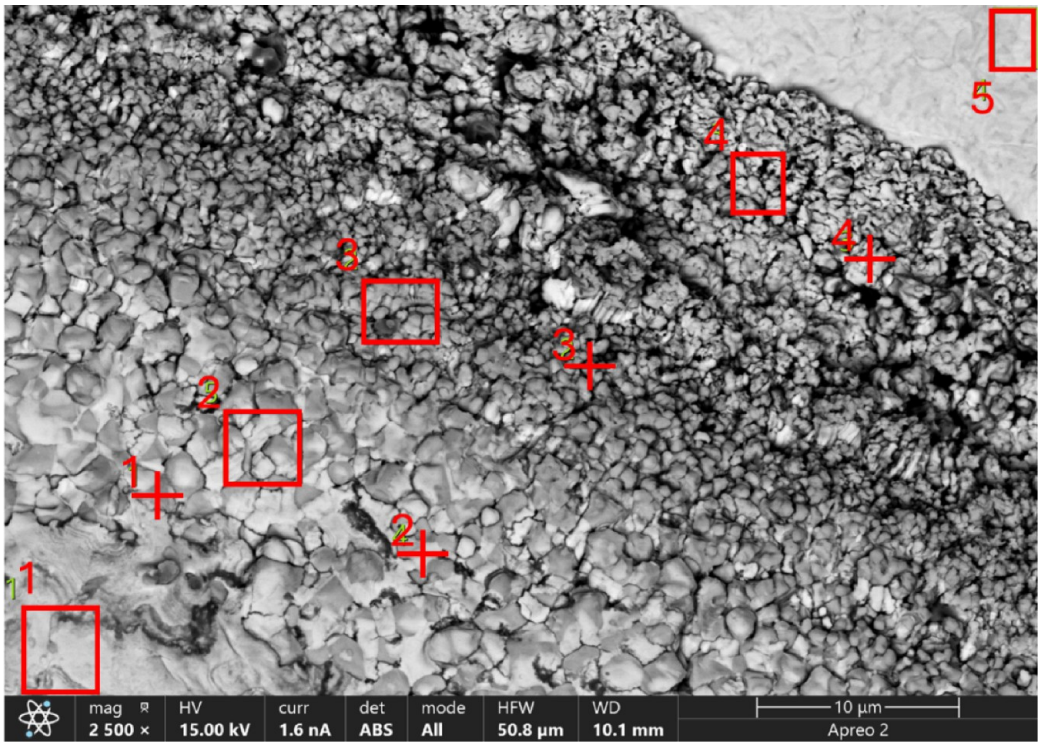

Figure 5. SEM/EDS spectral results and quantitative analysis of an InPb solder joint on Au after 1000 h at 125 °C in HV.

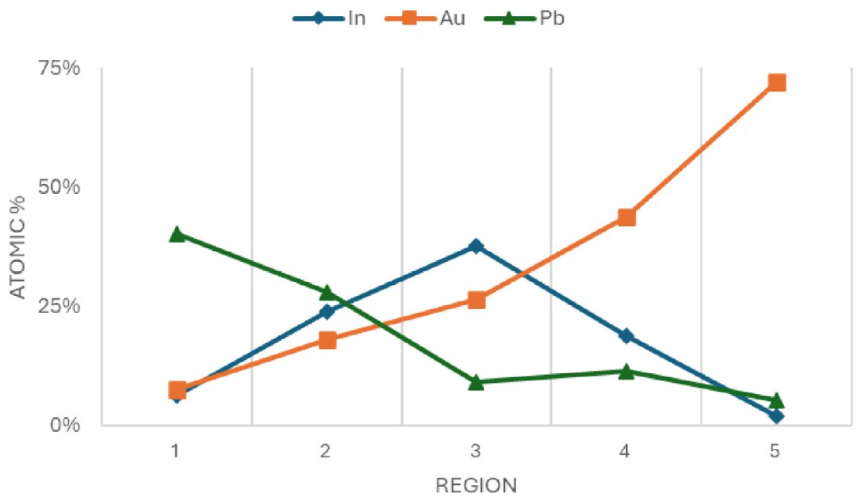

Figure 6. Line scan of the InPb solder joint on Au after 1000 h at 125 °C in HV.

The Arrhenius plot of the natural logarithm of the volume shrinkage rate K (in $\mu m^3\ h^{-1}$), i.e., $\ln(K)$ vs T^{-1}, is shown in Figure 9e. The plot has been fitted using eq 1 in which K_0 is the shrinkage rate at infinite temperature (extrapolated value). The graphical analysis yielded activation energy (E_a) values ranging from 0.38 to 0.41 eV (the detailed data are reported in Table 6).

$$\ln(K) = \ln(K_0) - \frac{E_a}{K_B T} \quad (1)$$

https://doi.org/10.1021/acsaelm.5c01580
ACS Appl. Electron. Mater. 2025, 7, 10161−10171

Table 2. Summary of Atomic % of InPb Solder Joint on Au after 1000 h at 125 °C

	Atomic %									
Element	Region 1	Region 2	Region 3	Region 4	Region 5	Point 1	Point 2	Point 3	Point 4	Point 5
C	3	3.7	6.3	5.3	4.4	3.2	1.2	2.4	2.3	2.4
O	38.7	26.8	19.5	18.8	14.3	21.5	24.7	24.9	17.2	14.1
In	22.4	31.7	19.7	37.3	5.7	24.8	40.7	38.6	20.3	8.6
Au	7.2	17.9	49.7	31.6	71.5	9.9	26	29.8	55	70.7
Pb	28.8	19.9	4.8	6.9	4.1	40.5	7.4	4.2	5.2	4.2
In:Au	3:1	2:1	1:3	1:1	1:13	3:1	2:1	1:1	1:3	1:8

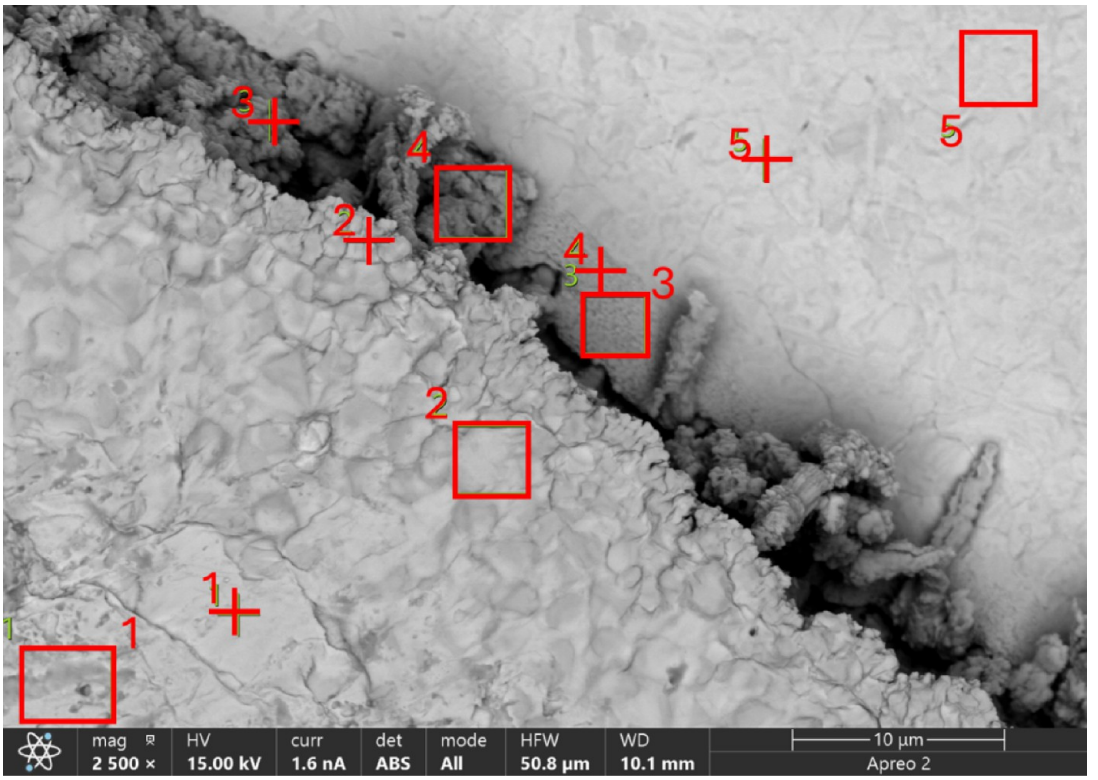

Figure 7. SEM/EDS spectral results and quantitative analysis of an InPb solder joint on Au after 1000 h at 125 °C.

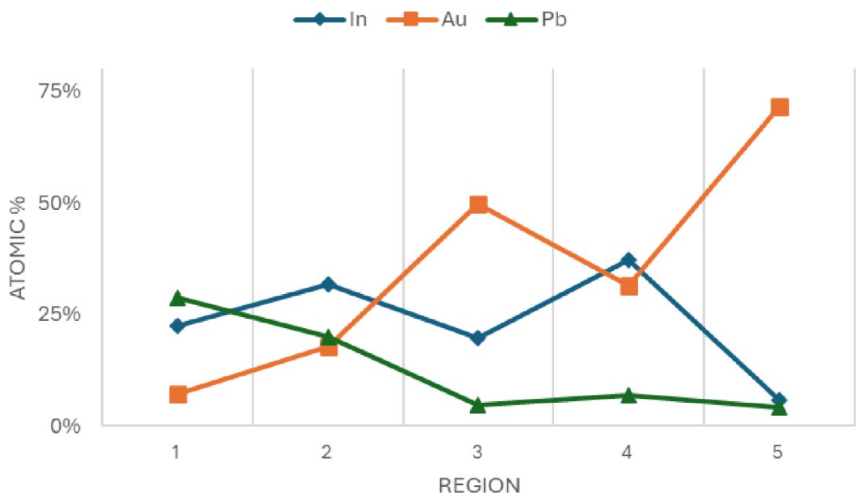

Figure 8. Line scan of the InPb solder joint on Au after 1000 h at 125 °C.

These shrinkage activation energies are comparable to those obtained for intermetallic compound growth in InPb/Au systems, with ∼0.45 eV for the silvery IMC and ∼0.21 eV for the black IMC, and the activation energy was found to be distributed in a narrow range (Yost et al. reported 0.61 eV[3]).

https://doi.org/10.1021/acsaelm.5c01580
ACS Appl. Electron. Mater. 2025, 7, 10161−10171

Table 3. Small Alloy (A) Volume Values over Aging Time at (A) 25°C, (B) 85°C, (C) 125 °C, and "Room Pressure"[a]

Alloy Volume/ Time	A at 25 °C [μm^3]	2σ	A at 85 °C [μm^3]	2σ	A at 125 °C [μm^3]	2σ
0	1.02×10^6	1.72%	1.07×10^6	1.72%	1.13×10^6	1.71%
250	1.02×10^6	1.72%	9.58×10^5	1.72%	9.86×10^5	1.72%
500	1.01×10^6	1.72%	8.82×10^5	1.73%	8.73×10^5	1.73%
1000	1.01×10^6	1.72%	8.22×10^5	1.73%	7.83×10^5	1.73%
V_R%	1%		23%		30%	

[a]Uncertainty 2σ is also reported as a relative percentage.

Table 4. Medium Alloy (B) Volume Values over Aging Time at (A) 25°C, (B) 85°C, (C) 125 °C, and "Room Pressure"[a]

Alloy Volume/ Time	B at 25 °C [μm^3]	2σ	B at 85 °C [μm^3]	2σ	B at 125 °C [μm^3]	2σ
0	4.64×10^6	1.50%	4.35×10^6	1.52%	5.32×10^6	1.46%
250	4.63×10^6	1.50%	4.08×10^6	1.54%	4.83×10^6	1.49%
500	4.61×10^6	1.50%	3.69×10^6	1.56%	4.30×10^6	1.52%
1000	4.59×10^6	1.50%	3.16×10^6	1.59%	3.69×10^6	1.56%
V_R%	1%		27%		31%	

[a]Uncertainty 2σ is also reported as a relative percentage.

Table 5. Big Alloy (C) Volume Values over Aging Time at (A) 25°C, (B) 85°C, (C) 125 °C, and "Room Pressure"[a]

Alloy Volume/ Time	C at 25 °C [μm^3]	2σ	C at 85 °C [μm^3]	2σ	C at 125 °C [μm^3]	2σ
0	1.94×10^7	0.62%	1.59×10^7	0.83%	1.40×10^7	0.94%
250	1.93×10^7	0.62%	1.50×10^7	0.88%	1.33×10^7	0.98%
500	1.93×10^7	0.62%	1.42×10^7	0.93%	1.24×10^7	1.04%
1000	1.93×10^7	0.62%	1.33×10^7	0.98%	1.14×10^7	1.10%
V_R%	1%		16%		29%	

[a]Uncertainty 2σ is also reported as a relative percentage.

This correspondence indicates that the volume reduction is closely linked to diffusion-driven IMC evolution during aging.

In addition, *AF*, defined as the ratio of the volume shrinkage rate K_T at two different temperatures, was calculated using eq 2:[16]

$$AF = \frac{K_{T2}}{K_{T1}} = \exp\left[\frac{E_a}{k_B}\left(\frac{1}{T_1} - \frac{1}{T_2}\right)\right] \quad (2)$$

where E_a is the activation energy, K_B is the Boltzmann constant, and T_1 and T_2 are the aging temperatures.

For the T_1 = 25 °C to T_2 = 125 °C range, *AF* = 57 for small alloys A and 42 for medium/large alloys B/C. This allows extrapolation to longer time scales. For A-group alloys, 100 h of aging at 125 °C is equivalent to 0.65 years at 25 °C, while 63 days at 125 °C correspond to 10 years at 25 °C. Also, for B and C alloy groups, 100 h at 125 °C corresponds to about 0.48 years at 25 °C, and 86 days at 125 °C correspond to 10 years at room temperature.

The evaluation of *AFs* is essential for the accurate prediction of long-term V_R in solder joints, a critical factor influencing joint reliability, particularly in space applications, where prolonged on-Earth storage at room temperature and controlled pressure conditions is required due to the time needed for the completion of satellite assembly before the space mission is launched. Given the requirement for extended terrestrial storage under controlled temperature and pressure before satellite assembly and launch, precise *AF* determination enables the prediction and validation of suitable safety factors under laboratory conditions, thereby ensuring the operational reliability of solder joints.

Another relevant aspect to be noted is the dependence of V_R as a function of the size of the solder joint. The ODM volume measurements indicate that junctions in the 200−400 μm range (A and B groups) show an average reduction in size by approximately 35% compared to larger 600 μm junctions (C group). This finding suggests that the parameter of surface area-to-volume ratio plays a critical role in InPb alloys. From a thermodynamic perspective, in correspondence with an interface, the two different phases in contact tend to assume shapes and have an extent of the surface area of contact that minimizes the surface tension of the interface and, consequently, the resulting free energy. This behavior leads to configurations with lower surface-to-volume ratios to reduce the overall interfacial energy and is consistent with the Gibbs−Thomson effect. This latter effect explains why the higher surface-to-volume ratio in smaller joints increases surface tension and raises the chemical potential of the various interfacial species, thus driving faster mass transport from the regions of small curvature. The greater surface tension accelerates V_R in smaller joints, as the system minimizes its free energy.

The evaluation of solder volume for SnPb/PtAu and SAC305/ENIG joints was performed with an ODM, as shown in Figure 10 for two alloys aged at 125 °C and at normal temperature. Results show the stability of the volume values for all adopted conditions of thermal aging. All the measured variations remained within the error margin of the instrument, confirming that no real volume change occurred over the aging time. This finding further demonstrates the morphological stability of both alloys, which withstand prolonged thermal aging without alteration. In addition, minimal IMC growth was observed. Tables 7 and 8 summarize the corresponding volume measurements for SnPb/PtAu and SAC305/ENIG solder joints, respectively.

The results clearly show that even after long-term thermal aging, the solder joints of SnPb/PtAu and SAC305/ENIG maintained a stable volume.

3.3. Pressure-Dependent Aging Behavior. To further investigate the impact of environmental conditions on the volume shrinkage phenomenon, we also examined the effects of pressure variations on aging by comparing samples at 125 °C under atmospheric pressure and at 125 °C in HV (1×10^{-6} mbar). We found that samples aged at 125 °C under atmospheric pressure showed greater V_R than those stored in HV (31% vs 16% after 1000 h, Figure 9f). Furthermore, from the ODM images, a significant difference in morphology was observed, stemming from the presence of dark rings appearing in the samples aged in vacuum, which are not observed in those aged at room pressure. This finding may be attributed to

https://doi.org/10.1021/acsaelm.5c01580
ACS Appl. Electron. Mater. 2025, 7, 10161−10171

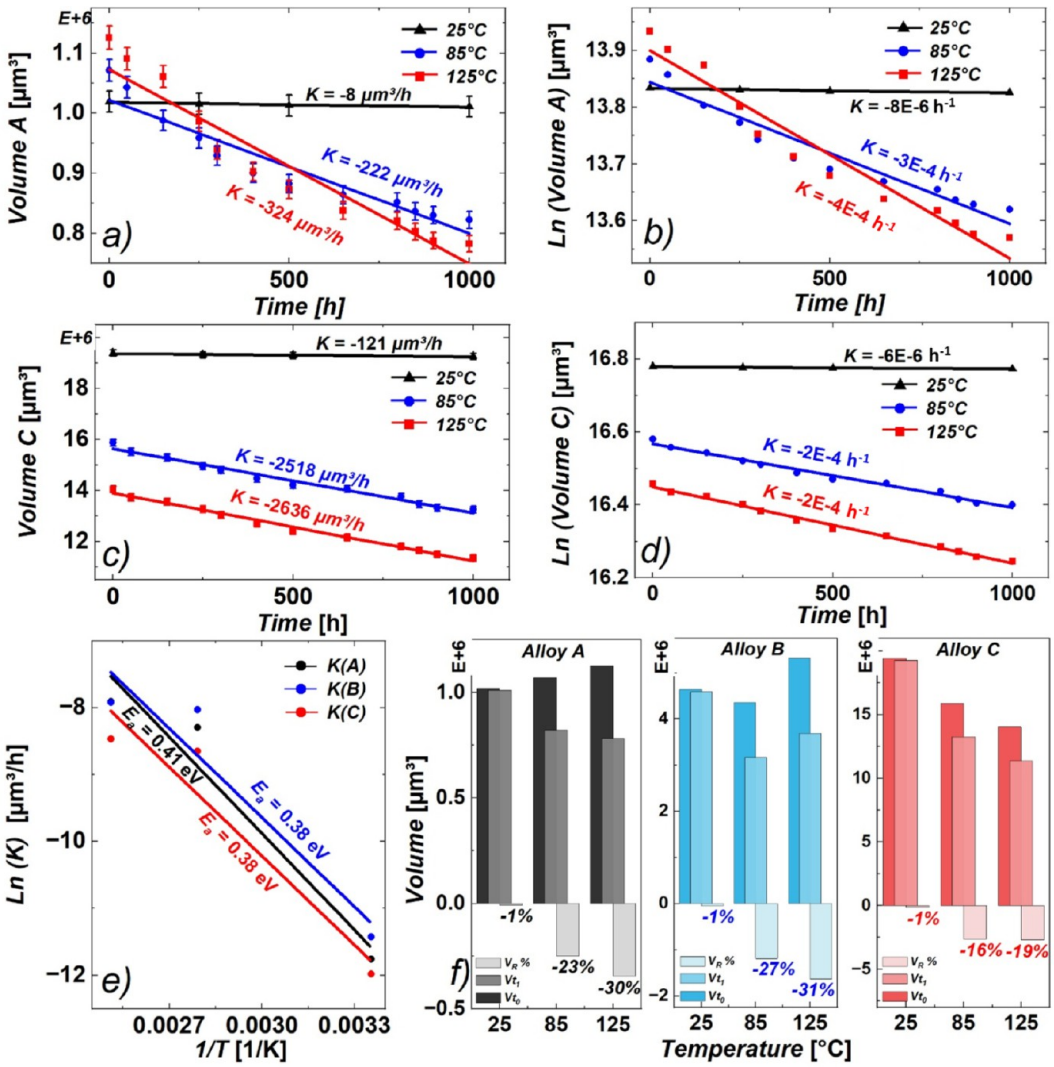

Figure 9. (a–d) Determination of the rate (K) of average volume (V) shrinking through graphical analysis of the plots: (a,c) V vs time and (b,d) ln(V) vs time. (e) Evaluation of the activation energy E_a for the volume shrinking process from the Arrhenius plot ln(K) vs T^{-1} considering the average volumes of samples A, B, and C. Plots (a) and (c) show the variations in the average volume of junctions A and C vs aging time, respectively. Plots (b) and (d) show the variations in the natural logarithm of the average volume of A and C vs aging time, respectively. (f) Comparative analysis of V_R and percentage change over 1000 h of aging time for different alloys and temperatures at room pressure.

Table 6. Arrhenius Data for the V_R Rates of Alloys A, B, and C at Different Temperatures[a]

T [°C]	$1/T$ [K^{-1}]	$-K$(A) [μm^3h^{-1}]	$-K$(B) [μm^3h^{-1}]	$-K$(C) [μm^3h^{-1}]	ln [$-K$(A)/μm^3h^{-1}]	ln [$-K$(B)/μm^3h^{-1}]	ln [$-K$(C)/μm^3h^{-1}]
25	3.3×10^{-3}	7.8×10^{-6}	1.1×10^{-5}	6.2×10^{-6}	−11.8	−11.4	−12.0
85	2.8×10^{-3}	2.5×10^{-4}	3.3×10^{-4}	1.7×10^{-4}	−8.3	−8.0	−8.7
125	2.5×10^{-3}	3.7×10^{-4}	3.6×10^{-4}	2.1×10^{-4}	−7.9	−7.9	−8.5

[a]The table includes the temperature values (T) in K, the reciprocal temperatures (T^{-1}) in K^{-1}, the rate constants with a minus sign ($-K$) in $\mu m^3/h$ for alloys A, B, and C, and the corresponding natural logarithms of the rate constants In($-K$). These data points are used in the Arrhenius plot for the calculation of E_a (Figure 9E).

a different evolution and outward propagation of the IMCs formed at the InPb–Au interface and along the joint edges.

Figure 11 provides a comprehensive view of the variations in volume as a function of aging time and pressure for solder joint groups A, B, and C. The enhanced volume shrinkage under atmospheric pressure suggests a synergistic effect between temperature and atmospheric components, possibly due to the occurrence of oxidation-assisted degradation. This chemical process might lead to the formation of solid-state oxidation products with higher density compared to the starting material, resulting in a consequent contraction of the total volume. By analyzing the full set of XRM images taken on three solder joints of each sample at t = 0 and 1000 h (see also Figure 2 for the profiles of $A2_{125\ °C\text{-air}}$ and $B2_{125\ °C\text{-air}}$), it is evident that porosity does not play any relevant role in the volume shrinkage reduction mechanism. This is because, at t = 0, the porosity is negligible (~0.5%) and increases over aging time up to ~1.5%, i.e., still a negligible value. If porosity had played any role, such a small increase of porosity would have led, in turn, to a volume enhancement instead of shrinkage. Therefore, the

https://doi.org/10.1021/acsaelm.5c01580
ACS Appl. Electron. Mater. 2025, 7, 10161–10171

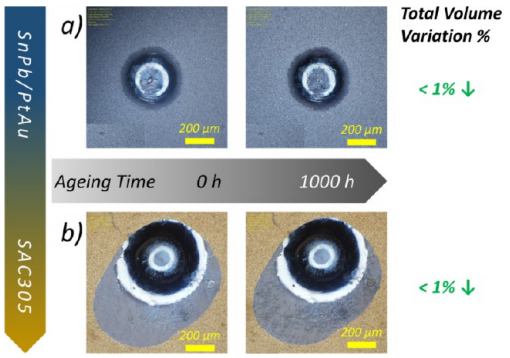

Figure 10. Morphological evolution and V_R% of SnPb/PtAu and SAC305/ENIG samples, analyzed via ODM, at 0 and 1000 h of aging under 125 °C: (a) SnPb/PtAu (B1) alloy and (b) SAC305/ENIG (B1) alloy. Both alloys show neither modification of morphology nor volume reduction.

origin of the shrinkage effect must be attributed to the eventual formation of intermetallic compounds (not to be considered as oxidative degradation products), which may result in a denser crystalline structure compared to that of the original solder alloy. The formation of an intermetallic species, consequent to the replacement of one type of metallic atom or the mixing/dispersing of microscopic crystals in a crystal with different types of metallic atoms, is generally favored by an increase in temperature when two distinct metallic phases are in contact. This is due to the associated increase of the entropic term when transitioning from distinct phases with net interfaces to an intermetallic intermediate phase with interpenetrating phases.[17] Moreover, the effect of shrinkage in a low-pressure environment resembling the ambient conditions of satellite operation cannot be ascribed to a sublimation effect with associated loss of mass, as this would have implied a uniform variation in volume for polycrystalline systems like the joint solders. However, the rate of shrinkage appears nonhomogeneous from the profiles of the sections shown in Figure 3.

Table 9 shows the degradation of the volume over aging time at different aging atmospheric pressures. The lower V_R% observed under HV is associated with the absence of oxidation and reduced interfacial reactions between In/Pb and residual oxygen. SEM/EDS spectral results and quantitative analysis confirmed minimal oxygen signals in HV-aged samples, while air-aged joints exhibited localized oxygen enrichment at the IMC/solder interface, as shown in Figures 5 and 7.

To support the proposed hypothesis, further microscopic and spectroscopic analyses shall be performed to clarify the origin of this phenomenon of shrinkage.

Although not fully understood, these observations highlight the critical role of both temperature and pressure in determining the stability of solder joints, with implications for predicting performance in varied environments, particularly in space applications where pressure changes dramatically from the Earth assembly step, the premission storage, to the mission itself.

For contrast, no detectable pressure dependence was exhibited by SnPb/PtAu and SAC305/ENIG solder joints. Their volumes, already reported in Tables 7 and 8 to be stable within experimental error in a high-vacuum environment, did not show detectable pressure dependence. This again emphasizes that pressure-sensitive shrinkage of InPb/Au is not a generic solder alloy behavior but a result of its intermetallic evolution, which is specific to it.

4. CONCLUSIONS

This study provides critical insights into the aging behavior of InPb/Au solder joints through nondestructive techniques such as XRM and ODM. A size-dependent volume reduction was observed, with smaller joints (~200−400 μm) exhibiting 35% greater volume shrinkage compared to larger ones (~600 μm), which can be compensated t_0 by increasing the solder alloy amount during the soldering process. Furthermore, atmospheric pressure was found to accelerate the aging process compared to high vacuum conditions, resulting in a volume reduction of 31% versus 16% after 1000 h at 125 °C. The calculated activation energies, ranging from 0.38 to 0.41 eV, enable reliable long-term performance predictions. These findings have immediate implications for enhancing electronic assembly processes in applications requiring high reliability, including space systems and dual-use technologies. The nondestructive approach adopted here allows for an in-depth investigation of dynamic processes in electronic materials, supporting the optimization of design and manufacturing strategies for next-generation assemblies. For instance, intentional oversizing of solder joint fillets during the assembly phase, based on a quantitative understanding of shrinkage kinetics and size-dependent effects, could significantly improve the long-term reliability of electronic systems in extreme environments. For comparison, SnPb/PtAu and SAC305/ENIG solder joints did not exhibit a measurable volume change under these same conditions, verifying their stable response and limited IMC growth. This indicates shrinkage as a distinctive property of InPb/Au solder joints. Further work at elevated temperatures and under changing pressure conditions is necessary to generalize these reliability predictions.

Overall, the results help to elucidate the mechanisms driving volumetric shrinkage, which is characteristic of the InPb/Au system, with a particular focus on the conditions under which intermetallic compounds form and their contribution to joint stability. These observations pave the way for new design strategies for electronic components intended for dual-use

Table 7. SnPb/PtAu Volume Measurement for Different Alloys over Aging Time at (A) 25°C, (B) 85°C, (C) 125 °C and "Room Pressure", and 125 °C HV[a]

Alloy Volume/Time	A2 at 25 °C [μm^3]	2σ	B2 at 85 °C [μm^3]	2σ	A2 at 125 °C [μm^3]	2σ	B2 at 125 $°C_{HV}$ [μm^3]	2σ
0	1.27×10^7	1.02%	1.20×10^7	1.06%	1.26×10^7	1.03%	1.27×10^7	1.02%
500	1.26×10^7	1.02%	1.20×10^7	1.06%	1.26×10^7	1.03%	1.26×10^7	1.03%
1000	1.26×10^7	1.02%	1.20×10^7	1.06%	1.26×10^7	1.03%	1.25×10^7	1.03%
1500	1.26×10^7	1.02%	1.20×10^7	1.06%	1.26×10^7	1.03%	1.26×10^7	1.02%
V_R%	1%		1%		0%		1%	

[a]The uncertainty 2σ is also reported as a relative percentage.

https://doi.org/10.1021/acsaelm.5c01580
ACS Appl. Electron. Mater. 2025, 7, 10161−10171

Table 8. Volume Measurement for SAC305/ENIG Different Alloys over Aging Time at (A) 25°C, (B) 85°C, (C) 125 °C and "Room Pressure", and 125 °C HV[a]

Alloy Volume/Time	B1 at 25 °C [μm^3]	2σ	B1 at 85 °C [μm^3]	2σ	B1 at 125 °C [μm^3]	2σ	B1 at 125 $°C_{HV}$ [μm^3]	2σ
0	1.91×10^7	0.63%	2.32×10^7	0.39%	1.80×10^7	0.70%	9.70×10^6	1.20%
500	1.91×10^7	0.64%	2.31×10^7	0.39%	1.80×10^7	0.70%	9.68×10^6	1.20%
V_R%	0%		0%		0%		0%	

[a]The uncertainty 2σ is also reported as a relative percentage.

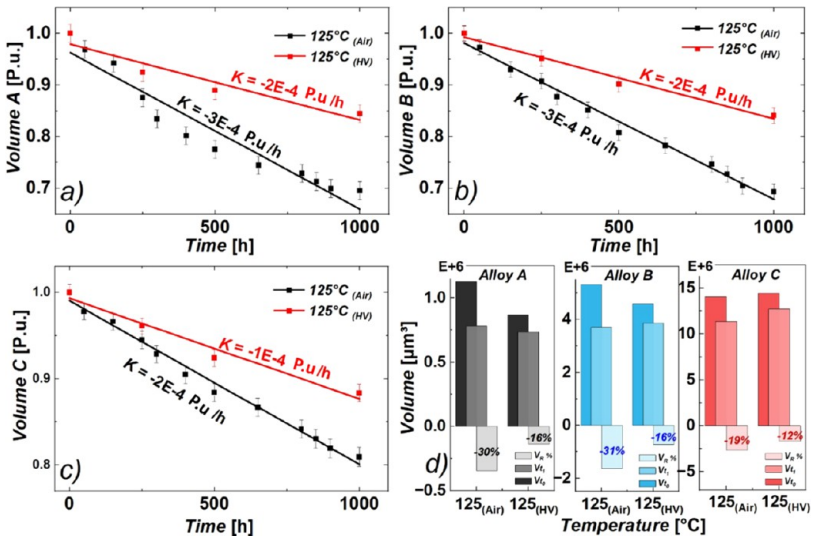

Figure 11. Analysis of V_R under different pressure conditions: Average volume (P_u) vs aging time for (a) A, (b) B, and (c) C junctions. (d) Comparison of V_R at t_0 and t_1 for different alloys and temperatures. Plots in (d) highlight the greater reduction of the solder joint volume under normal pressure conditions.

Table 9. Volume Values of Small and Large Size Alloys (Solder Samples A and C, Respectively) over Aging Time at (A) 125 °C and "Room Pressure", (B) 125 °C in HV

Alloy Volume/Time	A at 125 °C [μm^3]	A at 125 $°C_{HV}$ [μm^3]	C at 125 °C [μm^3]	C at 125 $°C_{HV}$ [μm^3]
0	1.13×10^6	8.70×10^5	1.40×10^7	1.44×10^7
500	8.73×10^5	7.74×10^5	1.24×10^7	1.33×10^7
1000	7.83×10^5	7.35×10^5	1.14×10^7	1.27×10^7
V_R%	33%	20%	23%	18%

systems, where robustness and reliability are critical to meet the demands of advanced civil and industrial applications.

AUTHOR INFORMATION

Corresponding Authors

Mirko Rocci − *Thales Alenia Space Italia, L'Aquila 67100, Italy*; Email: mirko.rocci@thalesaleniaspace.com

Danilo Dini − *CNIS Center, Università di Roma "La Sapienza", Roma 00185, Italy*; orcid.org/0000-0001-5005-4187; Email: danilo.dini@uniroma1.it

Authors

Mousa Al-Rbai'eh − *Thales Alenia Space Italia, L'Aquila 67100, Italy; CNIS Center, Università di Roma "La Sapienza", Roma 00185, Italy*; orcid.org/0009-0001-5947-955X

Simone Bandini − *Thales Alenia Space Italia, L'Aquila 67100, Italy; CNIS Center, Università di Roma "La Sapienza", Roma 00185, Italy*

Alessia Sanna − *CNIS Center, Università di Roma "La Sapienza", Roma 00185, Italy*

Luca Sollecchia − *Thales Alenia Space Italia, L'Aquila 67100, Italy*

Lorenzo Simone − *Thales Alenia Space Italia, L'Aquila 67100, Italy*

Marco Rossi − *CNIS Center, Università di Roma "La Sapienza", Roma 00185, Italy*

Complete contact information is available at: https://pubs.acs.org/10.1021/acsaelm.5c01580

Notes

The authors declare no competing financial interest.

ACKNOWLEDGMENTS

M.A.R. and S.B. performed the measurements and the data analysis. Mi.R. and M.A.R. wrote the main draft. Mi.R., D.D., and Ma.R. contributed to the interpretation of the results and critically reviewed the paper. Mi.R. conceived and supervised the work. All the authors discussed the results and revised the article. All authors have approved the final version of the manuscript. The authors gratefully acknowledge CNIS for providing access to advanced characterization instrumentation, partially funded through the ATOM project (Advanced Tomography and Microscopies, G11949), supported by Regione Lazio under the "*Open Infrastructure for Research*" program. M.A.R. acknowledges a themed PhD scholarship funded through the National Operational Program (PON) "Research and Innovation" 2014−2020 − Italian Ministry for Universities and Research (MUR) − and Thales Alenia Space Italia S.p.A. S.B. acknowledges a PhD Scholarship cofinanced

https://doi.org/10.1021/acsaelm.5c01580
ACS Appl. Electron. Mater. 2025, 7, 10161−10171

by Regione Lazio and Thales Alenia Space Italia S.p.A., within the framework of the Public Notice "Intervention for Strengthening Research in Lazio – Incentives for Innovation Doctorates for businesses".

REFERENCES

(1) Bastow, E. *Indium Corporation Tech Paper: Value Of InPb Solders*; Form No. 98830 R0, Indium Corporation, 2009.
(2) Dunn, B. D. *The Use of Indium Solder Alloys in Materials and Processes for Spacecraft and High Reliability Applications*; Springer Praxis Books: Switzerland, 2016; Vol. 6, pp. 363–369.
(3) Yost, F. G. Soldering To Gold Films: The Importance Of Lead-Indium Alloys. *Gold Bull.* **1977**, *10*, 94–100.
(4) Kessel, K.; *NEPP TRO Lead-Free Solder Body of Knowledge, TRO: Lead-free soldering NEPP Program Document*; 2005, pp. 1–12. https://nepp.nasa.gov/files/10977/Lead-Free%20Solder%20BOK%20Report%206-21-%202005.pdf.
(5) Li, Z.; Yang, Y.; Huang, W.; Gong, Y.; Pan, K. Study on IMC Growth Law of Solder Joints in Aerospace Electronic Products and Its Influence on Reliability. *J. Phys.: Conf. Ser.* **2023**, *2483*, 012017.
(6) Cheng, S.; Huang, C. M.; Pecht, M. A review of lead-free solders for electronics applications. *Microelectron. Reliab.* **2017**, *75*, 77–95.
(7) Chen, G.; Cui, X.; Wu, Y.; Li, W.; Wu, F. Performance of 96.5Sn–3Ag–0.5Cu/fullerene composite solder under isothermal ageing and high-current stressing. *Soldering Surf. Mount Technol.* **2021**, *33*, 35–46.
(8) Coyle, R.; Sweatman, K.; Arfaei, B. Thermal Fatigue Evaluation of Pb-Free Solder Joints: Results, Lessons Learned, and Future Trends. *JOM* **2015**, *67* (10), 2394–2415.
(9) Johansson, J.; Belov, I.; Johnson, E.; Dudek, R.; Leisner, P. Investigation on thermal fatigue of SnAgCu, Sn100C, and SnPbAg solder joints in varying temperature environments. *Microelectron. Reliab.* **2014**, *54*, 2523–2535.
(10) Rialland, J. F.; Perron, J. C. Viscosities of indium-lead liquid alloys. *Metall. Trans.* **1974**, *5*, 2401–2403.
(11) Yost, F. G.; Ganyard, F. P.; Karnowsky, M. M. Layer growth in Au-Pb/In solder joints. *Metall. Trans. A* **1976**, *7*, 1141–1148.
(12) Wang, C. Y.; Chen, Y. C.; Lee, C. C. Directly deposited fluxless lead-indium-gold composite solder. *IEEE Trans. Compon., Packag., Manuf. Technol.* **1993**, *16*, 789–793.
(13) Ma, L.; Bao, S.; Peng, J.; Du, Z. Failure Analysis of In/Au Solder Joints. In *Contribution presented at the 7th International Conference on Electronic Packaging Technology*; IEEE: Shanghai, China, 2006, pp. 1–4.
(14) Menzinger, M.; Wolfgang, R. The Meaning and Use of the Arrhenius Activation Energy. *Angew. Chem., Int. Ed.* **1969**, *8*, 438–444.
(15) Okamoto, H. Reevaluation of thermodynamic models for phase diagram evaluation. *J. Phase Equilib.* **1991**, *12*, 623–643.
(16) Chris South, P. E.Acceleration Factors and Life Predictions*International Symposium on Microelectronics*International Microelectronics Assembly and Packaging Society20201100–105
(17) Porter, D. A.; Easterling, K. E. *Phase transformations in metals and alloys*; 2nd ed.; Stanley Thornes Publishers Ltd: Cheltenham, UK, 2000.

https://doi.org/10.1021/acsaelm.5c01580
ACS Appl. Electron. Mater. 2025, 7, 10161–10171